Journal of
Micro/Nanolithography, MEMS, and MOEMS

SPIEDigitalLibrary.org/jm3

MOEMS deformable mirrors for focus control in vital microscopy

Mohammad J. Moghimi
B. Jeffrey Lutzenberger
Brant M. Kaylor
David L. Dickensheets

SPIE

MOEMS deformable mirrors for focus control in vital microscopy

Mohammad J. Moghimi
B. Jeffrey Lutzenberger
Montana State University
Electrical and Computer Engineering
530 Cobleigh Hall
Bozeman, Montana 59717

Brant M. Kaylor
Bridger Photonics, Inc.
2310 University Way, Building 4-4
Bozeman, Montana 59717

David L. Dickensheets
Montana State University
Electrical and Computer Engineering
530 Cobleigh Hall
Bozeman, Montana 59717
E-mail: davidd@ee.montana.edu

Abstract. Deformable membrane mirrors are promising MOEMS devices for focus control and aberration correction in vital microscopy, offering high speed focus adjustment in an optical system that can be miniaturized for *in vivo* use. This paper describes mirrors comprising metalized polymer membranes suspended over three concentric circular electrodes for electrostatic actuation. The membranes are 2-μm thick and 3 mm in diameter, made from the fully cross-linked photoset epoxy SU-8 2002. A layer of SU-8 2025 is used to establish a 30-μm thick air gap between the electrodes and the membrane mirror. The membranes are actuated by applying voltage to each electrode individually to achieve displacement as large as 12 μm while minimizing spherical aberration. Surface deflection is studied using phase-shift interferometry under both static and dynamic excitation. Using the deformable MOEMS mirror for focus control in an optical microscope we demonstrate the ability to adjust the location of the focal plane by 85 μm using an N.A. = 0.75 optical system. © *2011 Society of Photo-Optical Instrumentation Engineers (SPIE).* [DOI: 10.1117/1.3574129]

Subject terms: MOEMS; MEMS; membrane mirror; variable focus; spherical aberration; SU-8.

Paper 10077PR received Aug. 16, 2010; revised manuscript received Feb. 15, 2011; accepted for publication Mar. 7, 2011; published online Apr. 28, 2011; corrected May 20, 2011.

1 Introduction

Focus control is a persistent challenge for miniature instruments such as endoscopic or catheter-based imaging systems because of severe size constraints. Traditional methods based on motors and cams to move lens groups present problems in terms of size, power requirements and mechanical complexity that add to the overall size and cost of a miniaturized instrument. The slow speed of mechanized lens translation does not allow fast focus tracking.

An alternative approach to lens translation is the use of variable-power optics. Recent progress with both transmissive lenses and reflective lenses (curved mirrors) shows promise as means to achieve full-range focus control in miniature instruments. Examples of transmissive variable power lenses include MEMS pneumatic devices[1–6] and electrowetting lenses.[7,8] Such lenses can have a large range of optical power and are moderately fast (hundreds of hertz to a few kilohertz). Incorporation of fluids and pneumatic elements can introduce some complexity in the distal end of the probe, and to date little work has been done to demonstrate fine control of the aspheric constant for such lenses.

In contrast, electrostatic deformable membranes can provide fast (tens to hundreds of kilohertz) and precise focus control with an adjustable aspheric constant.[9–13] The footprint of such mirrors can be nearly as small as the mirror dimensions. The primary complexity introduced by these devices is accommodating a reflecting geometry. The major limitation, however, is the range of motion in deflection, or membrane stroke. Few electrostatic membranes have exceeded 10 μm of deflection, and most have demonstrated 5 μm or less. This has been simply too little stroke for focus adjustment that would address the fully available penetration depth achievable with *in vivo* confocal microsopy or optical coherence tomography.

We recently described a target for membrane mirrors for high N.A. microscopy: mirrors should be capable of 30 μm of deflection while controlling spherical aberration out to at least the fifth order (surface shape varying as r^6).[14] Such a mirror would provide 200-μm focus adjustment at N.A. = 0.9 in tissue, comprising an appreciable portion of the penetration depth for this imaging modality.

This paper describes new progress toward that goal using mirrors made from a compliant material (the photoset epoxy SU-8 2002) and designed specifically for focus control. We describe mirrors capable of at least a 12-μm stroke, and demonstrate their use in a microscope with N.A. = 0.75, with a focus control range of 85 μm. With future improvements similar mirrors are expected to achieve this 30-μm deflection target for high N.A. microscopy applications.

2 Device Fabrication

The SU-8 focus control mirror is fabricated using three photomasks in a die-bonded process as shown in Fig. 1. Aluminum control electrodes are patterned on an oxidized silicon wafer called the spacer wafer. Then, 30 μm of SU-8 2025 (Microchem, Inc.) is deposited and patterned to form the spacer. The spacer establishes an air gap beneath the membrane mirror, and defines the shape of the mirror's perimeter. These focus control mirrors have a circular membrane boundary and are designed for focusing a beam that is incident normal to the surface. Air channels in the spacer layer allow airflow into and out of the space under the membrane. An image of a completed spacer and electrodes is shown

1932-5150/2011/$25.00 © 2011 SPIE

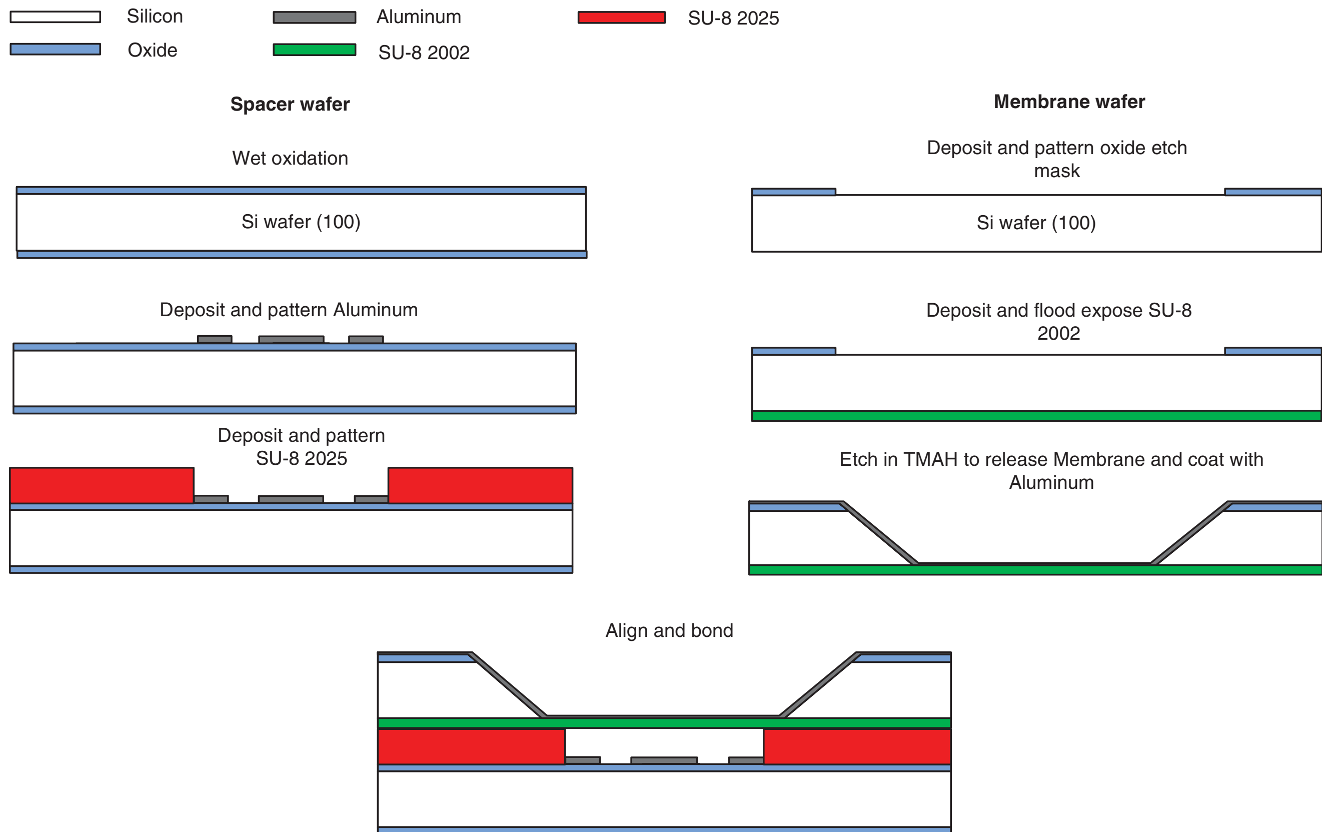

Fig. 1 Fabrication sequence for the variable focus membrane mirror.

in Fig. 2(a). The spacer wafer is diced and cleaned prior to bonding to the membrane die.

The membrane wafer is a single side polished (100) wafer. It is oxidized and then patterned on the back side to define etch windows for a subsequent through-wafer etch to create free-standing membranes. The membrane layer is 2 μm of SU-8 2002, spun on the polished side of the wafer to create a flat membrane. After a prebake at 95°C the wafer is flood-exposed to crosslink the SU-8 layer and then hard-baked at 200°C for 90 min. The membranes are released by etching through the wafer in tetramethyl ammonium hydrocide (TMAH) with concentration 12.5% at temperature 75°C. A single-side etching apparatus is employed to minimize contact between the SU-8 membrane layer and the TMAH etchant. Some membrane dies ruptured or wrinkled during the release step but more than 80% of devices ended up with flat membranes. Surface quality of the released SU-8 membrane is good, with no visible roughness. The fully released membrane wafer is coated with 200 nm aluminum on the back side to provide the optical reflecting surface and is then diced and cleaned. Finally, the membrane die is aligned and bonded to the spacer die, with the SU-8 membrane in contact with the SU-8 spacer. Approximate alignment is sufficient, since the width of the free membrane is approximately 5 mm, while the spacer opening is 3 mm. Overall die size is approximately 10×10 mm. The bonded die are mounted on an 8-pin SOIC to DIP adapter as shown in Fig. 2(b). An aluminum wire bonder is employed to make electrical connection between the control electrodes and 8-pin SOIC. A conductive epoxy creates the connection between reflective aluminum on the membrane and the ground electrode.

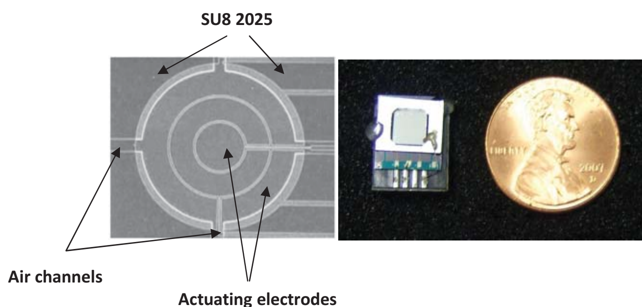

Fig. 2 (a) A completed spacer overlaying actuation electrode. (b) An assembled mirror. Finished die size is approximately 1 cm^2.

3 Device Characterization

3.1 *Mechanical Properties*

The membrane mirrors have been characterized under both static and dynamic electrical excitation. Figure 3 shows displacement measured at the membrane center versus applied voltage. For this measurement, the voltage on all three actuation electrodes was the same. Deflection was measured using an optical interferometer. Membrane in-plane tension can be estimated by fitting the displacement data to the theoretical displacement using a simple membrane model,[15]

$$T\nabla^2 s(r) + p(r) = \rho \frac{\partial^2 s}{\partial t^2},$$

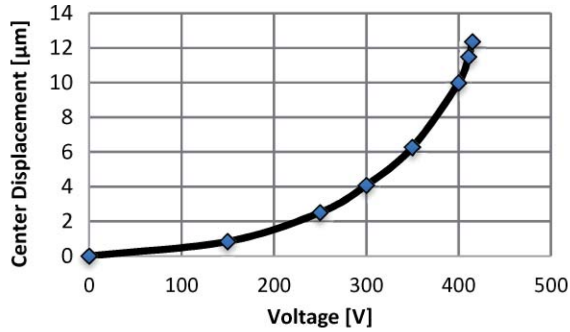

Fig. 3 Static deflection as a function of applied voltage.

where p is the electrostatic pressure, $T = h\sigma$ is the in-plane tension, h is the membrane thickness of 2 μm, σ is the residual stress, and ρ is the area mass density for SU-8 2002, which is $(1.2\times10^3\ h)$ kg/m^2. Residual stress is a function of the thermal history of the membranes, with particular dependence on the hardbake conditions. For our membranes we find residual stress to vary from approximately 14 to 33 MPa, with the membrane shown in Fig. 2 exhibiting a residual stress of 30 MPa. The influence of process parameters and device aging on the final membrane stress remains a topic of investigation in our laboratory, as controlling this parameter is important for the manufacturability of focus control devices using this material.

Maximum deflection is limited by electrostatic pull-in. All results presented in this paper are for open-loop actuation, and maximum useable displacement with an air gap of 30 μm is approximately 12 μm. The pull-in voltage is measured as 440 V.

3.2 *Frequency Response*

The membrane frequency response was also measured using stroboscopic interferometry, for small signal sinusoidal excitation. In this method, the light source is a pulsed laser synchronized with the electrical drive signal, to obtain static interference images of a vibrating membrane. The phase of the strobe pulse is varied while measuring the deflection magnitude determined from the fringe images.[16] Both mechanical response magnitude and phase can be determined by this method. The results are plotted in Fig. 4 for the same membrane characterized above for dc deflection. The mirror exhibits a bandwidth of 100 Hz before the response begins to decline. However, measureable deflection persists (diminished by approximately 20 dB) at frequencies up to 50 kHz. Examining the phase response we find the frequency corresponding to 90° phase lag to be between 30 and 40 kHz. This compares favorably with the predicted frequency of the first mechanical resonance[15] $f_0 = (2.405/2\pi r_0)\sqrt{T/\rho} = 40$ kHz using $\sigma = 30$ MPa as determined from the deflection data in Sec. 3.1 and $r_o = 1.5\times10^{-3}$ m for the membrane radius. We tentatively attribute the low overall bandwidth and deviation from a simple second order system to air damping effects, but we have not yet studied this effect and further experiments and modeling are warranted to explain the observed dynamic behavior.

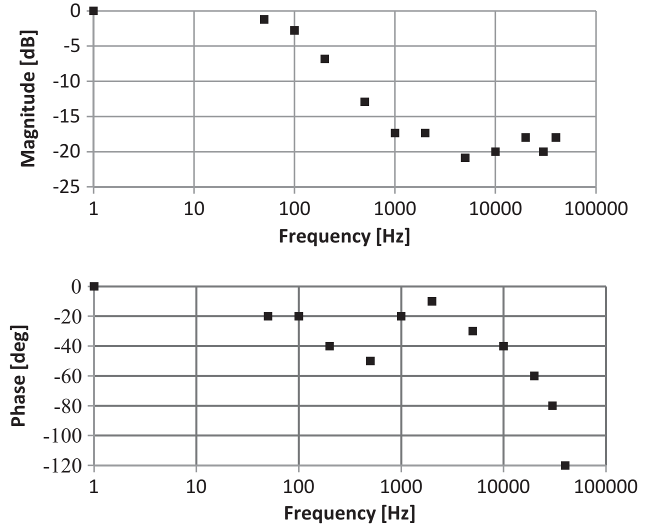

Fig. 4 Small signal response to sinusoidal driving voltage with a dc offset. Membrane diameter is 3 mm, and the air gap is approximately 30 μm.

3.3 *Optical Properties*

Optical properties of the membrane are critical for its usefulness as a variable focus element. Surface quality of the membrane is excellent, since the mirror surface is the interface between the polished membrane wafer and the spin-coated SU-8. Mirror flatness and aberrations during deflection depend on stress uniformity in the membrane, uniformity of the air gap beneath the membrane, alignment of the electrodes to the membrane mechanical boundary, the presence of particles in the air gap, and particles between the bonded die that cause separation between the membrane and the supporting spacer. To quantify the aberrations on the mirror we have performed a modal decomposition of the mirror surface shape using Zernike polynomials, which are orthogonal on the unit disk. It is customary to present the coefficients of these terms as a "Zernike spectrum," but the details of the polynomial normalization and the order of the terms in the spectrum are not standardized. We have adopted the polynomials and mapping used by Fricker in his MATLAB routine ZERNFUN2.m,[18] specified in Table 1. The first column identifies the mode number, and the last column identifies the common name for these low order aberrations.

Figure 5 shows a surface profile made using phase-shift interferometry for a 2-mm diameter membrane with no applied voltage, showing its baseline surface height variation. The raw height information is shown in the upper left of Fig. 5. The colorbar scale indicates height in nanometers. Coefficients for the best fit Zernike polynomials are indicated in the upper right of Fig. 5. The units for the coefficients in the Zernike spectrum are also nanometers. The lower left of Fig. 5 shows the surface height data with tilt and offset removed and the lower right of Fig. 5 shows the residual aberration after subtracting tilt, offset, and parabolic curvature. The residual aberration therefore refers to the mirror surface height error relative to the best-fit paraboloid of revolution. Peak to valley residual aberration is 591 nm for this device, with rms aberration of 56 nm.

Table 1 Zernike polynomials associated with terms 1 to 15 in the Zernike mode spectrum.

Term No.	n,m for Z_n^m	Polynomial	pk-pk amplitude	Aberration type
1	0,0	1	-	piston
2	1,-1	$r\cos(\theta)$	1	tilt about y-axis
3	1,1	$r\sin(\theta)$	1	tilt about x-axis
4	2,-2	$r^2\cos(2\theta)$	1	astigmatism
5	2,0	$2r^2-1$	2	defocus
6	2,2	$r^2\sin(2\theta)$	1	astigmatism
7	3,-3	$r^3\cos(3\theta)$	1	trefoil
8	3,-1	$(3r^3-2r^2)\cos(\theta)$	1.13	coma
9	3,1	$(3r^3-2r^2)\sin(\theta)$	1.13	coma
10	3,3	$r^3\sin(3\theta)$	1	trefoil
11	4,-4	$r^4\cos(4\theta)$	1	quadrafoil
12	4,-2	$(4r^4-3r^2)\cos(2\theta)$	1.13	2nd astigmatism
13	4,0	$6r^4-6r^2+1$	1.5	spherical
14	4,2	$(4r^4-3r^2)\sin(2\theta)$	1.13	2nd astigmatism
15	4,4	$r^4\sin(4\theta)$	1	quadrafoil

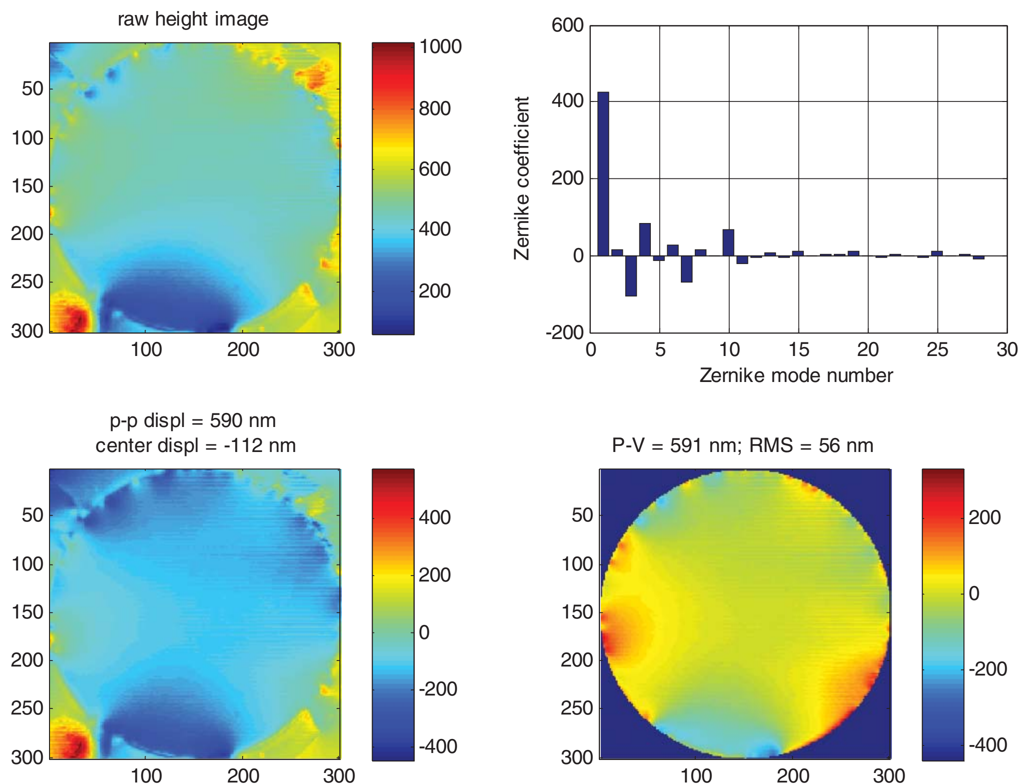

Fig. 5 A 2-mm diameter membrane mirror measured at rest, using a phase shift interferometer. The raw surface height map (upper left), coefficients for the best fit Zernike polynomials (upper right), the surface height map with tilt and offset removed (lower left) and the residual aberration after subtracting tilt, offset and parabolic curvature (lower right) are shown. Units for all surface height maps and the Zernike spectrum are nm. The Zernike mode polynomials are identified in Table 1.

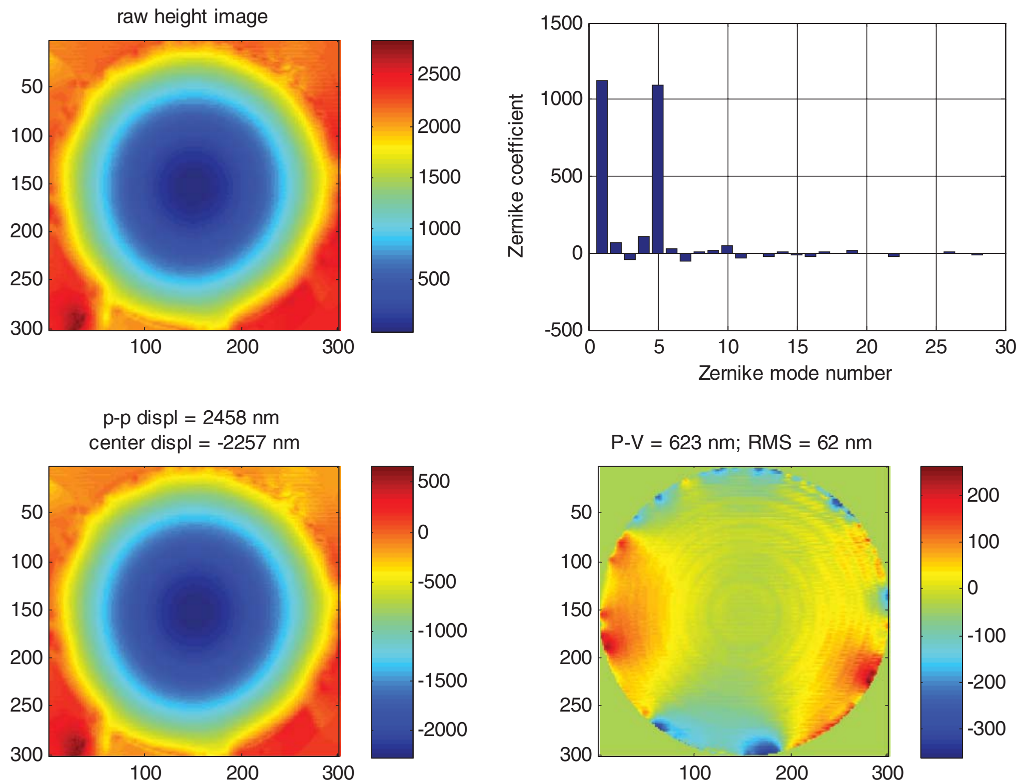

Fig. 6 The same mirror as shown in Figure 5, with 300 V applied to all three actuation electrodes. The figure shows the raw surface height map (upper left), coefficients for the best fit Zernike polynomials (upper right), the surface height map with tilt and offset removed (lower left) and the residual aberration after subtracting tilt, offset and parabolic curvature (lower right). Units for all surface height maps and the Zernike spectrum are in nanometers. The Zernike mode polynomials are identified in Table 1.

The dominant surface errors are astigmatism, corresponding to Zernike terms 4 and 6, and trefoil, corresponding to terms 7 and 10. The pk-pk variation for each of these terms remains less than 100 nm. These aberrations may arise from asymmetry in the in-plane stress introduced during device assembly. Due to particles preventing perfect contact between the two die, an initial separation exists between the membrane layer and the spacer layer when the die are bonded together. After the membrane and spacer die are mechanically joined, the membrane is brought into contact with the spacer SU-8 layer with electrostatic force, causing the two to laminate and remain in contact after subsequent removal of the voltage. We hypothesize that this is a possible source of nonuniformity and initial deformation of the membrane. We hope to address this error with improvements in the bonding process in the future.

Figure 6 shows the same surface profile data with a uniform voltage of 300 V across the membrane. The dominant Zernike term is now defocus (term 5), corresponding to a mirror radius of curvature of approximately 225 mm and focal length of 113 mm. The residual aberration with piston, tilt, and defocus removed is only slightly worse than the

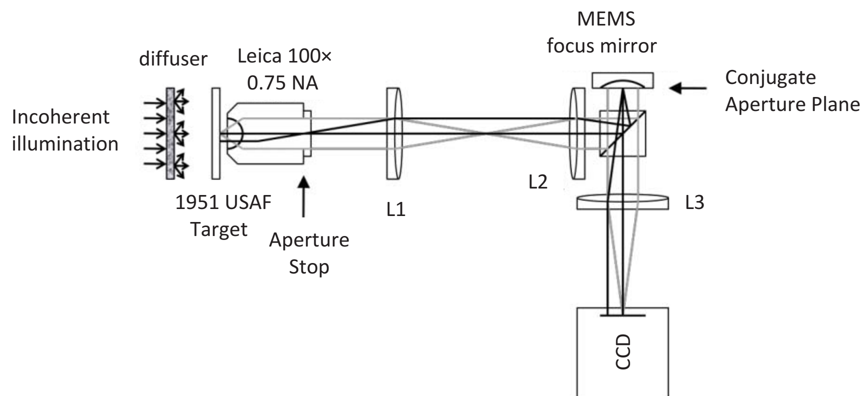

Fig. 7 Imaging setup to demonstrate focus control with the MOEMS mirror. Objective lens N.A. is 0.75, while the system magnification is 75×.

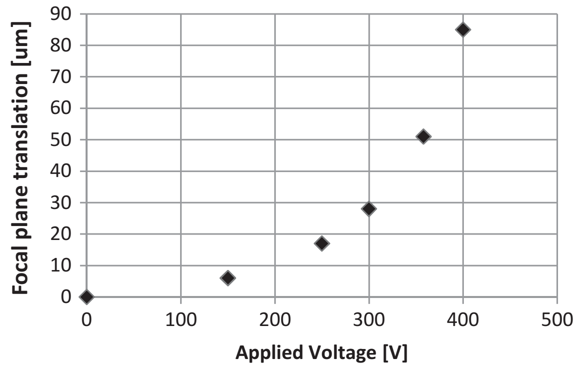

Fig. 8 Displacement of focal plane from its nominal position as a function of voltage on the MOEMS mirror.

resting case, measuring 623 nm peak-to-valley and 62 nm rms. Additionally, the magnitude of the Zernike coefficients excluding defocus have not increased.

4 Imaging Demonstration

We are developing MOEMS membrane mirrors to provide focus and aberration control for high N.A. imaging systems. One application for such devices is miniaturized microscopes for endoscopic imaging. The advantage of a variable focus membrane optic is high speed, the elimination of motors and mechanical linkages needed to translate fixed focus lenses, and the ability to compensate for focus-dependent spherical aberration arising from the fixed optics or the tissue itself.

Toward that goal we assembled an imaging system operating at N.A. = 0.75 with a MOEMS mirror for focus control. The setup is illustrated in Fig. 7. A transparent object is illuminated from the left with incoherent illumination. The imaging lens was a Leica 100×0.75 N.A. microscope objective with 2-mm focal length and a 3-mm diameter exit pupil. A 1:1 telescope comprising achromatic lenses L1 and L2 (100-mm focal length) relays the beam to the MOEMS mirror, where the MOEMS mirror plane is conjugate to the exit pupil of the objective lens. A beamsplitter is used to separate the beam reflected from the MOEMS mirror, and achromatic lens L3 (150-mm focal length) forms an image on a CCD camera. The magnification of the system is $150/2 = 75$.

For our imaging demonstration we used a 3-mm diameter mirror. The minimum radius of curvature (corresponding to maximum membrane deflection) was measured with a uniform voltage of 415 V to be 94 mm, yielding a focal length for the concave mirror of 47 mm. For the imaging demonstration we limited the control voltage to 400 V. We measured the position of best focus as a function of control voltage on the MOEMS mirror by translating the object until the best image was obtained. Figure 8 shows the change in location of the focal plane versus applied voltage. The full range of focus control was 85 μm at maximum applied voltage of 400 V.

Figure 9 shows images of a 1951 USAF resolution target for different locations of the focal plane. The three targets shown are from group 7, elements 4, 5 and 6. The smallest bars are 228 line pairs per mm. Figure 9(a) shows a reference image with the MOEMS mirror replaced with an optical mirror. Figure 9(b) is the corresponding image with 0 V on the membrane. Some astigmatism is observed in the image, with an axial translation of approximately 2 μm between the horizontal and vertical focal planes, but the smallest bars are clearly resolved with good contrast. Figure 9(c) shows the image after application of 350 V and a translation of the object 50 μm, while Fig. 9(d) shows the image with 400 V on the mirror and the object translated 85 μm. In the last image

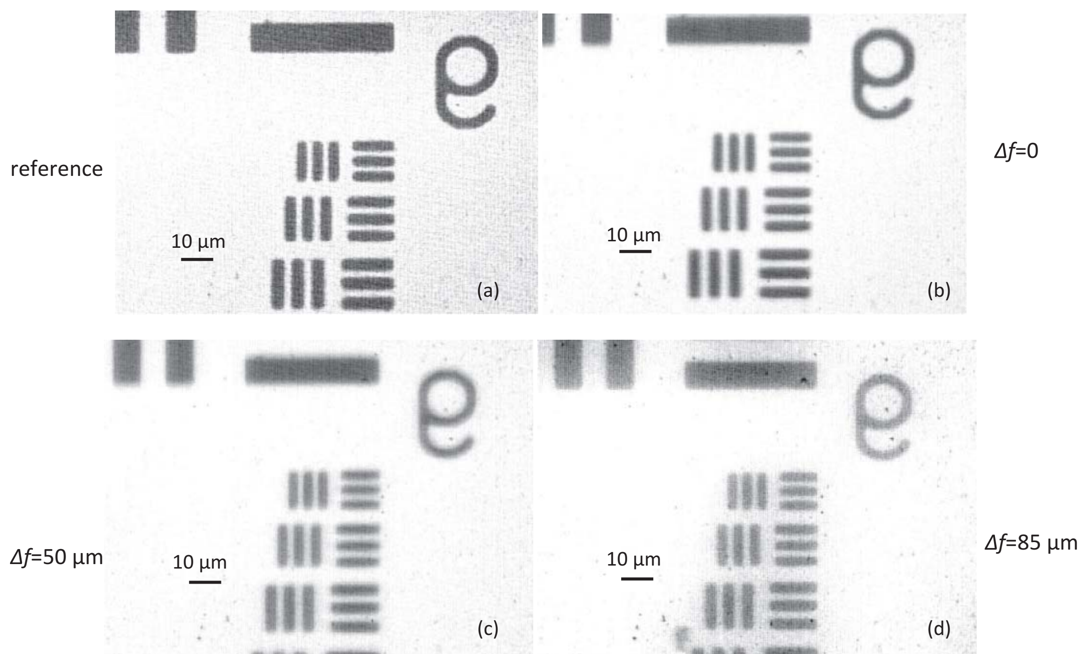

Fig. 9 Images of USAF resolution target, group 7 elements 4–6. (a) Reference image made with a flat mirror in place of the MOEMS mirror; (b) 0 V on the MOEMS mirror, and no focus adjustment; (c) 350 V on the MOEMS mirror, with the target translated 50 μm closer to the objective lens; and (d) 400 V on the MOEMS mirror, with the target translated 85 μm from the nominal focal position.

the bars in group 7 element 6 are clearly resolved, but there is some loss of contrast that we attribute to uncompensated spherical aberration introduced by the objective lens when the image plane is translated away from the design working distance.

5 Discussion

These results represent significant progress toward realizing a variable focus device able to adjust over the full accessible imaging depth (typically 150 to 200 μm) when imaging tissue using confocal microscopy at high numerical aperture.[14] Nevertheless, several improvements are possible that should result in future membrane mirrors with a greater range of focus control and still lower residual aberration in the focused beam as well as higher speed operation. The limitation to large displacement is a practical upper limit to the voltage that can be applied to these devices before electrical breakdown occurs in the device or the air gap. We do not observe electrical breakdown for these devices at voltages as high as 415 V, but we do not yet know the practical limit. The use of position sensing and feedback control has been demonstrated to produce stable displacement beyond the snap-down point, and also to allow a "soft" snapdown that reduces the voltage when the membrane does ultimately snap down to the substrate.[17] Closed loop control of these membranes could lead to an improvement in displacement by a factor of 2, with an attendant doubling of the range of focus control, without further increase in actuation voltage. Improvements in the bonding process should promote membrane initial flatness and reduce the residual aberration. SU-8 process improvements should reduce the residual stress which, at 30 MPa, is significantly larger than the range of 15 to 20 MPa that has been reported in the literature.[19] Lowering the residual stress reduces the tension in the membrane, resulting in greater deflection at maximum electric field strength. Finally, improvement in the design for better air flow and reduced damping should extend the frequency response of future membranes.

As the range of focus control increases, the demands on the mirror to correct spherical aberration increase. Two sources of spherical aberration are the variable depth of tissue into which the beam penetrates as focus is adjusted, and the aberration of the imaging optics that change as the location of the focal plane is adjusted. This latter source of aberration may be dominant, especially at very high numerical aperture. Future mirrors may need to be capable of not only many tens of micrometers of displacement stroke, but also the correction of several waves of spherical aberration that may include terms of high order. Full optical simulation will be necessary in these high N.A. systems to establish the prescription of a variable focus optic necessary to achieve high fidelity imaging throughout the range of focus.

6 Conclusions

We have demonstrated the feasibility of making focus control mirrors from large (3-mm diameter) free standing SU-8 2002 membranes that are deflected using electrostatic actuation. We achieved a stroke in excess of 12 μm using a mirror with an air gap of 30 μm, using 415 V for the actuation voltage. Initial imaging demonstrations have shown the ability to adjust the location of the focal plane by 85 μm in air, using an N.A. = 0.75 optical system.

Acknowledgments

This project was supported by the National Science Foundation under Project No. DBR-0754608 and IIP-0810778, and the Montana Board of Research and Commercialization Technology Grant No. 09-28. The device was fabricated at the Montana Microfabrication Facility at Montana State University.

References

1. K.-H. Jeong, G. Liu, N. Chronis, and L. Lee, "Tunable microdoublet lens array," *Opt. Express* **12**(11), 2494–2500 (2004).
2. D. Mader, A. Seifert, and H. Zappe, "Fabrication of aberration-corrected tunable micro-lenses," *International Conference on Optical MEMs and Nanophotonics, IEEE/LEOS*, Freiburg, Germany, pp. 60–61 (2008).
3. P. M. Moran, S. Dharmatilleke, A. H. Khaw, K. W. Tan, M. L. Chan, and I. Rodriguez, "Fluidic lenses with variable focal length," *Appl. Phys. Lett.* **88**(4), 041120 (2006).
4. H. Oku, and M. Ishikawa, "High-speed liquid lens with 2 ms response and 80.3 nm root-mean-square wavefront error," *Appl. Phys. Lett.* **94**(22), 221108 (2009).
5. H. Ren, D. Fox, P. A. Anderson, B. Wu, and S.-T. Wu, "Tunable-focus liquid lens controlled using a servo motor," *Opt. Express* **14**(18), 8031–8036 (2006).
6. A. Werber and H. Zappe, "Tunable pneumatic microoptics," *J. Microelectromech. Syst.* **17**(5), 1218–1227 (2008).
7. B. Berge and J. Peseux, "Variable focal lens controlled by an external voltage: An application of electrowetting," *The European Physical Journal E: Soft Matter and Biological Physics* **3**(2), 159–163 (2000).
8. S. Kuiper and B. H. W. Hendriks, "Variable-focus liquid lens for miniature cameras," *Appl. Phys. Lett.* **85**(7), 1128–1130 (2004).
9. P. A. Himmer and D. L. Dickensheets, "Spherical aberration correction using a silicon nitride deformable membrane mirror," *IEEE /LEOS Optical MEMS 2005: International Conference on Optical MEMS and Their Applications*, pp. 185–186 (2005).
10. P. A. Himmer, D. L. Dickensheets, and R. A. Friholm, "Micromachined silicon nitride deformable mirrors for focus control," *Opt. Lett.* **26**(16), 1280–1282 (2001).
11. J. Mansell, and R. Byer, "Micromachined silicon deformable mirror," *Proc. SPIE* **3353**, 896 (1998).
12. U. M. Mescheder, C. Estañ, G. Somogyi, and M. Freudenreich, "Distortion optimized focusing mirror device with large aperture," *Sens. Actuators, A* **130–131**, 20–27 (2006).
13. G. Vdovin, P. M. Sarro, and S. Middelhoek, "Technology and applications of micromachined adaptive mirrors," *J. Micromech. Microeng.* **9**(2), R8–R20 (1999).
14. D. L. Dickensheets, "Requirements of MEMS membrane mirrors for focus adjustment and aberration correction in endoscopic confocal and optical coherence tomography imaging instruments," *J. Micro/Nanolith. MEMS MOEMS* **7**(2), 021008 (2008).
15. K. F. Graff, "*Wave Motion in Elastic Solids*," Dover Publications, Inc. Mineola, NY (1991).
16. C. Rembe, and R. S. Muller, "Measurment system for full tree-dimensional motion charactrization of MEMS,"*J. Microelectromech. Syst.* **11**(5), (2002).
17. S. J. Lukes, P. A. Himmer, E. J. Moog, S. R. Shaw, and D. L. Dickensheets, "Feedback-stabilized deformable membrane mirrors for focus control," *J. Micro/Nanolith. MEMS MOEMS* **8**(4), 043040 (2009).
18. P. Fricker, *Zernike Polynomials* (18 May 2005, Updated 11 Mar 2008) (http://www.mathworks.com/matlabcentral/fileexchange/7687-zernike-polynomials), MATLAB Central File Exchange. Retrieved November, 2010.
19. S. Keller, G. Blagoi, M. Lillemose, D. Haefliger, and A. Boisen, "Processing of thin SU-8 films," *J. Micromech. Microeng.* **18**, 125020 (2008).

Mohammad J. Moghimi received his degree BS in electrical engineering from K. N. Toosi University of Technology, Tehran, Iran in 2005 and his MS, degree in electrical engineering from Amirkabir University of Technology, Tehran, Iran in 2008. He is currently a PhD student developing new MEMS devices and fabrication techniques especially for micro-optical components at Montana State University, Bozeman, Montana.

B. Jeffrey Lutzenberger received his BS and MS degrees in civil engineering from Montana State University. He received his PhD degree from Montana State University in 2005. His research interests include numerical modeling and microfabrication techniques. His current research focuses on the use of microfabrication techniques to miniaturize optical systems for biomedical imaging applications.

Brant M. Kaylor received his BS degree in optics from the University of Rochester in 2002 and his MS degree in optical sciences from the University of Arizona in 2004. He joined Bridger Photonics, Inc. as an optical scientist in 2008. His research interests include biomedical imaging systems, feature specific imaging and compressive sensing, pattern and image recognition, and 3D imaging.

David L. Dickensheets received his PhD degree in electrical engineering from Stanford University in 1997. From 1996 to 1997 he was a research associate in the Edward L. Ginzton Laboratory at Stanford University. In 1997, he joined the faculty at Montana State University in Bozeman, where he is currently a professor of electrical engineering. His research interests include optical imaging and spectroscopy of tissues, and the application of microfabrication technologies to develop miniature optical instruments for biomedical and industrial imaging applications, telecommunications, and planetary exploration.